

a restoring time constant of 5 months for the surface temperature¹⁶, a collapse of NADW formation induced by the introduction of a large negative salinity anomaly in the North Atlantic leads also to enhanced ventilation of the thermocline with fresher water (with signal propagation by coastal and equatorial Kelvin and Rossby waves within less than three decades from the Atlantic through the Indian Ocean to the northeast Pacific). However, this mechanism (compare ref. 6) accounts for only about one-third of the radiocarbon signal in the OAGCM. The remaining part thus can be explained by effects caused by changes in the atmosphere.

Although there is some agreement between model and geological data for circulation changes along the American west coast, there are also some disagreements. The cooling near the coast in our model is rather small (~1 K), whereas sediment records suggest^{6,29} a surface cooling of 2–3 K. Because there is some discrepancy between alkenone-based and foraminifera-based (*Globigerina pachyderma*) SST estimates for the Last Glacial Maximum from the Santa Barbara basin^{6,29}, and *G. pachyderma* may have a subsurface habitat³⁰, the upwelling 'discrepancies' may not necessarily reflect model inadequacies. The large changes in land ice cover, which are not included in our simulations, would also influence the circulation response. Another important shortcoming of the simulations is the coarse resolution (both horizontally and vertically) which makes the comparison with local phenomena in regions with large topography gradients questionable and does not allow the simulation of several important small-scale features. To address the above discrepancies a more complete set of experiments would be required with fully realistic boundary conditions for the deglacial.

Despite the differences mentioned above, our results clearly demonstrate the influence of variations in NADW formation on the North Pacific. In the case of a collapse of NADW formation, both the atmospheric and oceanic transmission of the signal lead to enhanced ventilation of the northeast Pacific thermocline, with the atmospheric effect about twice as strong as the oceanic. These results explain concurrent changes in the North Atlantic and North Pacific for both the Younger Dryas and (possibly) earlier millennial-scale cooling events of a similar nature^{9–12}. Owing to the atmospheric teleconnection, a cooling in the North Atlantic and increased sea-ice cover alone seem to be sufficient to enhance thermocline variation in the northeast Pacific. □

Received 30 September 1996; accepted 2 April 1997.

- Heusser, C. J. *Late Pleistocene Environments of North Pacific and North America* (Spec. Publ. 35, Geogr. Soc., New York, 1960).
- Peteet, D. M. & Mann, D. H. Late-glacial vegetation, tephra, and climatic history of southwestern Kodiak Island, Alaska. *Ecoscience* 1, 255–267 (1994).
- Peteet, D. M. Global Younger Dryas? *Quat. Int.* 38, 93–104 (1995).
- Kallel, N. *et al.* Evidence of cooling during the Younger Dryas in the western North Pacific. *Oceanol. Acta* 11, 369–375 (1988).
- Keigwin, L. D. & Jones, G. A. Deglacial climatic oscillations in the Gulf of California. *Paleoceanography* 5, 1009–1023 (1990).
- Kennett, J. P. & Ingram, B. L. A 20,000-year record of ocean circulation and climate change from the Santa Barbara Basin. *Nature* 377, 510–514 (1995).
- van Geen, A. *et al.* Ventilation changes in the northeast Pacific during the last deglaciation. *Paleoceanography* 11, 519–528 (1996).
- Thunell, R. C. & Mortyn, P. G. Glacial climate instability in the Northeast Pacific Ocean. *Nature* 376, 504–506 (1995).
- Behl, R. J. & Kennett, J. P. Brief interstadial events in the Santa Barbara Basin, NE Pacific, during the past 60 kyr. *Nature* 379, 243–246 (1996).
- Kotilainen, A. T. & Shackleton, N. J. Rapid climate variability in the North Pacific during the past 95,000 years. *Nature* 377, 323–326 (1995).
- Benson, L. V. *et al.* Climatic and hydrologic oscillations in the Owens Lake Basin and adjacent Sierra Nevada, California. *Science* 274, 746–749 (1996).
- Phillips, F. M. *et al.* Chronology for fluctuations in Late Pleistocene Sierra Nevada glaciers and lakes. *Science* 274, 749–751 (1996).
- Rooth, C. Hydrology and ocean circulation. *Prog. Oceanogr.* 11, 131–149 (1982).
- Maier-Reimer, E. & Mikolajewicz, U. In *Oceanography 1988* (eds Ayala-Castañares, A., Wooster, W. & Yáñez-Arancibia, A.) 87–100 (UNAM, Mexico, 1989).
- Rahmstorf, S. Bifurcations of the Atlantic thermohaline circulation in response to changes in the hydrological cycle. *Nature* 378, 145–149 (1995).
- Mikolajewicz, U. & Maier-Reimer, E. Mixed boundary conditions in ocean general circulation models and their influence on the stability of the model's conveyor-belt. *J. Geophys. Res.* 99, 22633–22644 (1994).
- Manabe, S. & Stouffer, R. J. Simulation of abrupt climate change induced by freshwater input to the North Atlantic Ocean. *Nature* 378, 165–167 (1995).
- Schiller, A., Mikolajewicz, U. & Voss, R. The stability of the North Atlantic thermohaline circulation in a coupled ocean-atmosphere general circulation model. *Clim. Dyn.* (in the press).

- Manabe, S. & Stouffer, R. J. Two stable equilibria of a coupled ocean-atmosphere model. *J. Clim.* 1, 941–866 (1988).
- Wright, D. G. & Stocker, T. F. *Ice in the Climate System* (ed. Peltier, W. R.) 395–416 (Springer, Berlin, 1993).
- Stocker, T. F. & Wright, D. G. Rapid changes in ocean circulation and atmospheric radiocarbon. *Paleoceanography* 11, 773–795 (1996).
- Roeckner, E. *et al.* Simulation of the present-day climate with the ECHAM model: impact of model physics and resolution. (Tech. Rep. No 93, Max-Planck-Inst. für Meteorologie, Hamburg, 1992).
- Maier-Reimer, E., Mikolajewicz, U. & Hasselmann, K. Mean circulation of the LSG OGCM and its sensitivity to the thermohaline surface forcing. *J. Phys. Oceanogr.* 23, 731–757 (1993).
- Voss, R. & Sausen, R. Techniques for asynchronous and periodically synchronous coupling of atmosphere and ocean models. Part II: impact of variability. *Clim. Dyn.* 12, 605–614 (1996).
- Voss, R., Sausen, R. & Cubasch, U. Periodically synchronously coupled integrations with the atmosphere-ocean general circulation model ECHAM3/LSG. *Clim. Dyn.* (submitted).
- Fairbanks, R. G. A 17,000-year glacio-eustatic sea level record: influence of glacial melting rates on the Younger Dryas event and deep-ocean circulation. *Nature* 342, 637–642 (1989).
- Goslar, T. *et al.* High concentration of atmospheric ¹⁴C during the Younger Dryas cold episode. *Nature* 377, 414–417 (1995).
- Mikolajewicz, U. A meltwater induced collapse of the 'conveyor belt' thermohaline circulation and its influence on the distribution of ¹⁴C and ¹⁸O in the oceans. (Tech. Rep. 189, Max-Planck-Inst. für Meteorologie, Hamburg, 1996).
- Herbert, T. D., Yasuda, M. & Burnett, C. Glacial-interglacial sea-surface temperature record inferred from alkenone unsaturation indices, site 893, Santa Barbara Basin. *Proc. ODP* 146 (pt 2), 257–264 (1995).
- Sautter, L. R. & Thunell, R. C. Seasonal variability in the ¹⁸O and ¹³C of planktonic foraminifera from an upwelling environment: Sediment trap results from the San Pedro Basin, Southern California Bight. *Paleoceanography* 6, 307–334 (1991).

Acknowledgements. We thank T. Herbert, L. Keigwin, E. Maier-Reimer, T. Stocker and L. Stott for discussions. T.J.C. was supported by the US NSF.

Correspondence should be addressed to U.M. (e-mail: mikolajewicz@dkrz.de).

Catastrophic collapse at stratovolcanoes induced by gradual volcano spreading

B. van Wyk de Vries & P. W. Francis

Department of Earth Sciences, The Open University, Walton Hall, Milton Keynes, UK

Unlike ordinary mountains, which are formed by slow uplift and erosion, volcanoes are constructed rapidly. As a consequence, many are liable to massive flank failures, leading to debris avalanches (for example, at Mount St Helens in 1980). Such failures occur worldwide about once every 25 years (ref. 1) and even small ones can present a major hazard—in particular if far-reaching tsunamis are generated, as at Mayu-yama in 1792 (ref. 2). Previous work has tended to emphasize differences in eruption style associated with flank failure², but here we focus on the fundamental structural causes of failure. Most volcanic failures are generated by magmatic intrusion and flank spreading³. We present evidence, however, that Mombacho volcano in Nicaragua experienced a previously unrecognized type of failure, triggered by sub-volcanic basement spreading. Notably, collapses related to basement spreading do not require that the volcano be magmatically active, and thus flank failure may pose a significant risk even at inactive volcanoes, which are rarely monitored.

Mombacho volcano rises 1,400 m above the west shores of Lake Nicaragua, on a basement of Quaternary ignimbrite of the Las Sierras Formation^{4,5} (Fig. 1). Conspicuous debris avalanche deposits on two sides of the volcano provide unequivocal evidence for recent flank failure. One deposit, below a well defined collapse scar, forms the remarkable Las Isletas archipelago in Lake Nicaragua (Fig. 1). The other, on the south side below the deep 'El Crater' scar, covers ~60 km² with hummocky avalanche deposit (Fig. 2). Forest cover indicates that the avalanche deposits are at least 1,000 years old. The 20,000-yr-old Apoyo pumice underlies the deposits, giving a maximum age⁶.

Volcano spreading provides a framework to interpret the structural and magmatic evolution of volcanoes^{7–9}. We propose here a new failure mode caused by lateral displacement of sub-volcanic strata. A similar process has been proposed for the Hawaiian shield

volcanoes¹⁰ but remains controversial^{11,12}, in part because of the lack of physical evidence for the involvement of basement material. Our observations lend weight to the hypothesis, although we stress the differences in scale and geological context: Mombacho is a small standard stratocone, whereas Hawaii is a large oceanic shield complex. In particular, the thickness of the proposed weak layer at Hawaii is a small fraction (1%) of the volcano height⁷, and acts purely as a slip plane on which internal deformation of the volcano flank is accommodated. At Mombacho, the weak layer thickness is ~20% of the volcano height and it is deformation taking place *within* this layer that causes failure of the overlying edifice.

Earlier work suggested that the radial basement spreading limited the hazard of flank failure at volcanoes⁴, but here we argue that spreading on a restricted sector initiated the Las Isletas failure. In contrast, the El Crater failure resulted from progressive hydrothermal weakening of the cone and consequential flank spreading. Evidence for explosive activity in the form of tephra layers, pyroclastic flow deposits or juvenile fragments is absent from both the Las Isletas and El Crater deposits. This emphasises that flank failure can occur without associated magmatic activity.

The presence of large amounts of Las Sierras ignimbrite within the Las Isletas avalanche deposit demonstrates that the failure involved basement, because these ignimbrites underlie the volcano. The Las Sierras material comprises the central and lowermost parts of the deposit, adjacent to a shallow basin forming the Aseses inlet (Figs 1 and 2). A small scarp extending from the eastern wall to the lake indicates that the failure margin reached the lake here. This suggests that the failure plane cut into basement under Aseses beyond the volcano foot. An analogous situation occurs at Socompa, North Chile, where a debris avalanche deposit contains 60% basement¹³ and the failure margin extends 5 km from the volcano^{13,14}. Blocks of Las Sierras ignimbrite have pervasive calcite-cemented shear fractures, quite distinct from the open, spaced fractures associated with avalanche disaggregation, and consistent with deformation before failure. Thrusting along the north base and slumping of the southeastern side⁴ provide additional evidence of slow basement deformation (Fig. 2). Thus before collapse took place, the north and east base of Mombacho was spreading outwards. This preferential direction of spreading may reflect localized lake sediment layers within the Las Sierras Formation, though these were not identified in the deposit. Alternatively, the orientation of spreading structures could have been controlled by regional stress, which in Nicaragua promotes east-west extension and north-south compression¹⁵.

The floor of the collapse scar slopes at a similar angle to the cone surface, suggesting that the avalanche slid along a bedding plane (Fig. 3). In this respect, Las Isletas resembles many dip-slope slides and avalanches, both volcanic and non-volcanic^{16,17}, but it also has a lower part extending into the basement. The combination of dip-slope upper slide and a lower spreading sector could have developed into the avalanche in the way shown in Fig. 3a. Thrust anticline growth at the front of the spreading sector elevates the front of the spreading sector, so that basement can be included in a subsequent failure without excessively deep excavation (Fig. 3a).

The model implies that spreading is integral to the development of failure and demonstrates that identification of spreading is an important first step in assessing potential collapse hazard. Furthermore, in contrast to radially spreading volcanoes⁴, preferential spreading in one direction is critical to collapse development: whereas radial spreading tends to generate inward-dipping graben which inhibit collapse⁸, sector spreading (as at Mombacho) generates failure-prone outward-dipping structures (Fig. 3b). Spreading in a preferential direction may be caused by buttressing⁸, by the regional slope of basement beds, by regional stress¹⁵, by weak basement or by high fluid pressures under one side. Importantly, hot springs in the Aseses inlet suggest a possible role for elevated pore pressures (Fig. 2).

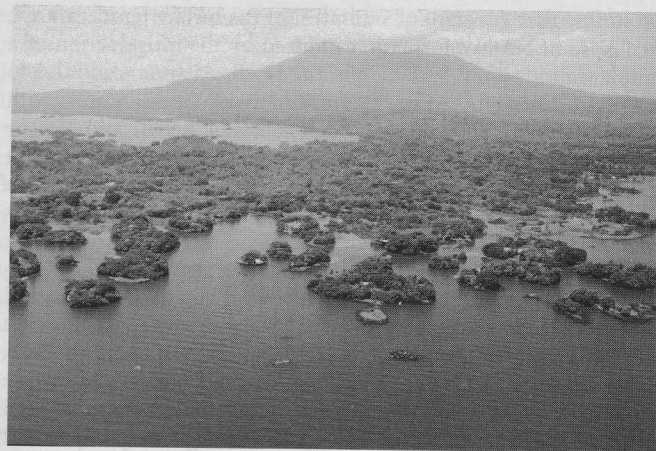


Figure 1 View of the Las Isletas collapse deposit at Mombacho. The islands of the archipelago are the distal part of the avalanche deposit and are composed of basement Las Sierras ignimbrite with a veneer of rocks from the volcano above. The basement ignimbrites were excavated from the Aseses embayment seen in the middle ground. They slope from 150 m above sea level on the western side of Mombacho to about sea level in the area of the photograph: a dip of ~2° (ref. 4). There are no confirmed reports of historic eruptions at Mombacho²⁵.

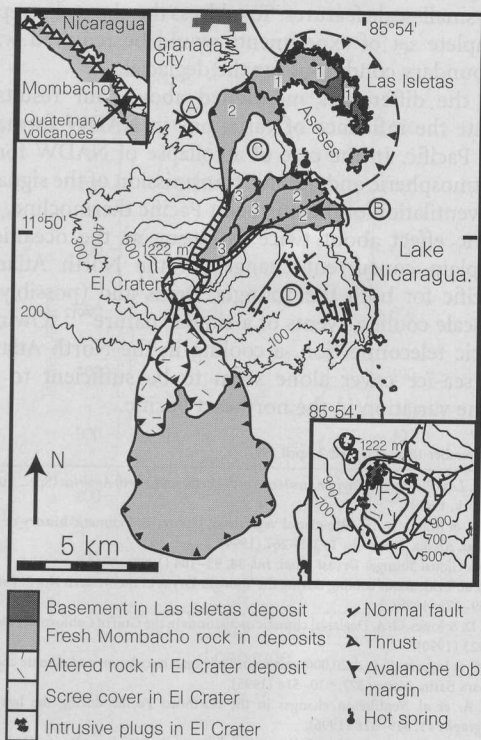


Figure 2 Geological map of Mombacho, showing the two recent flank failures and debris avalanche deposits of Las Isletas and El Crater. Insets show location of Mombacho and a detail of El Crater. Points on map draw attention to: A, thrusting observed at north base⁴; B, scarp in Las Isletas deposit indicating buried failure margin extending down into basement; C, La Calera post-collapse lava flow; D, normal faults resulting from spreading of the southeastern flank. Fumarole field in El Crater shown by black circle at F. Numbers in Las Isletas deposit indicate sequential emplacement of lobes by retrogressive collapse. Within the central lobe which forms the Las Isletas archipelago (1), the Las Sierras facies forms the lowest material, partially covered by fresh lava blocks. By contrast, the overlying marginal lobes are composed entirely of fresh cone material (2). Small secondary lobes overlie the La Calera lava flow, erupted in the scar after the collapse (3), and one large headwall segment still awaits collapse.

In contrast to Las Isletas, the El Crater collapse scar is at least 400 m above the sub-volcanic basement, so failure clearly took place wholly within the cone. The proximal avalanche deposit is composed of thick lobes of a chaotic mixture of hydrothermal clays, altered lava and scoria. Buttresses on the walls of the scar are plugs of basalt and andesite, in places highly altered. Below one of these there is a vigorous fumarole field. A zone of intense alteration extends over much of the lower crater, the material being similar to that in the avalanche. Progressive alteration of the volcano core, converting

strong volcanic and intrusive rock to weak hydrothermal clays¹⁸, probably caused collapse (Fig. 3c)¹⁹.

Because hydrothermal weakening is progressive, deformation of affected volcanoes is likely to begin long before failure, as in other deep-seated failures¹⁷, and would be indicated by steepening and thrusting of the lower flank and by normal faulting higher up. Increased fluid pressure²⁰ and magma intrusion could accelerate failure, with pre-existing mass creep controlling the failure direction. Swanson²¹ suggested such a relationship between old altered domes, and the orientation of the Mt St Helens collapse.

Precursory slow spreading probably triggered flank failures at other volcanoes, notably Socoma¹⁴. Probable precursory spreading has already been detected at Colima²² and Etna²³, and we postulate future failures for other volcanoes currently exhibiting evidence of active spreading (Fig. 4). Spreading features observed at Kilauea may be sites of potential collapse, though the direct involvement of the basal décollement in such events is still uncertain¹⁰⁻¹².

Because the features described here are produced by gradual processes, they may be detectable long before any failure occurs. Identification of basement and flank spreading allows prediction of the type and location of potential collapses and assessment of their probable effects. Potential collapses can be detected from evidence of individual spreading sectors (Fig. 4a), while the symptoms of flank spreading will be bulging and fracturing (Fig. 4b), core weakening by persistent fumarolic activity, and evidence of old domes and plugs. At Mt St Helens, where collapse was immediately preceded by considerable deformation²⁴, evidence of previous flank movement in the collapse scar²¹ suggests that if the north flank had been monitored before 1980, the location of the ultimate collapse could have been identified well before the recent activity.

Once the location and structure of potential collapses are recognized, deformation monitoring can determine baseline rates of spreading activity, which probably range from 1 to 50 cm yr⁻¹

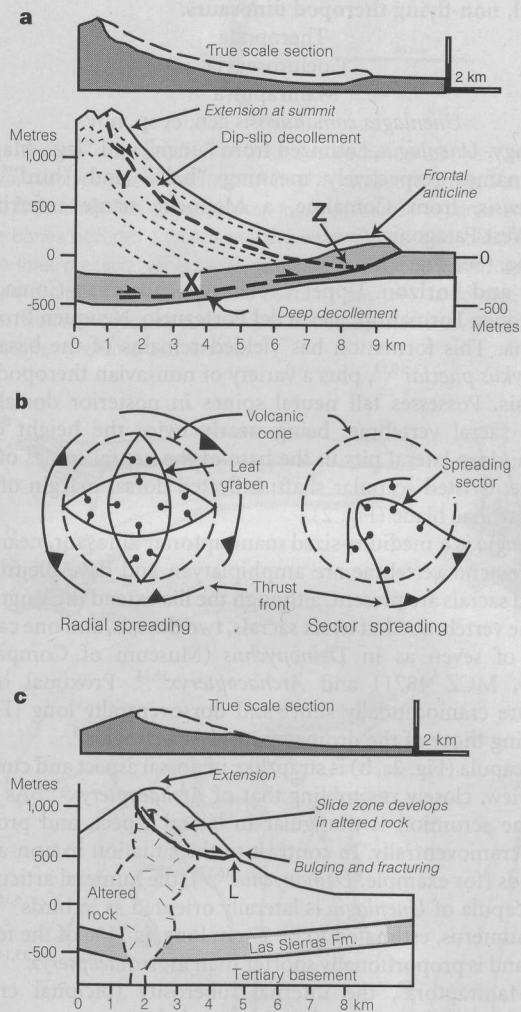


Figure 3 Interpretation of spreading and collapse structures at Mombacho, showing contrasting models for basement failure at Las Isletas (**a** and **b**), El Crater (**c**) and probable precursory features. **a**, Las Isletas: basement collapse. Deep spreading on decollement (X) within the Las Sierras Formation rises to produce a frontal anticline at the foot of Mombacho. Spreading induces differential movements within the upper parts of the volcano⁴, contributing to the initiation of slip on a plane (Y) within the cone. Once the dip-slip decollement is activated, the mass above it places additional load on the spreading front, inducing increased movement, and eventual failure through the frontal anticline (Z). **b**, Plan diagrams illustrating the difference in structural style between a radially spreading and a sector spreading volcano (that is, Mombacho). Radial spreading produces inward dipping normal faults that cut any potential failure plane in the cone^{4,8}. In contrast, sector spreading creates outward dipping faults, which promote collapse. **c**, El Crater: flank collapse. The El Crater collapse crater is ~1.5 km wide and long, and 700 m deep. Its walls curve inwards toward the opening, where there is a pronounced 30-m-high lip (L). Overall, the shape is that of a rotational slump failure in a mechanically homogenous medium¹⁷, so no pre-existing decollement plane is required. Such failures usually begin when shear strength is reduced over a wide area^{17,26}. At El Crater this homogeneous strength loss was produced by progressive hydrothermal alteration.

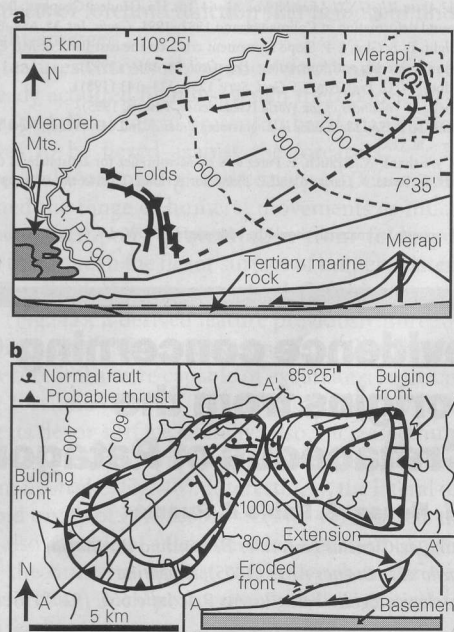


Figure 4 Examples of potential failures at spreading volcanoes. **a**, A spreading sector with collapse potential: Merapi, Java; a long sector is spreading. Drawn after van Bemmelen⁹. The compressive front is restrained by the Menoreh mountains. This barrier may have inhibited flank failure during a rapid spreading stage before a major eruption⁹. **b**, A spreading flank with collapse potential: Orosi, Costa Rica; two flank sectors are creeping outwards. Each has a steepened front just above the cone foot, probably hosting a thrust, and a crescent-shaped graben higher up.

(refs 4, 9), and unusual accelerations which may immediately precede collapse can be detected. Hundreds of volcanoes are potentially liable to collapse: prediction of future collapse sites depends on their timely identification by the criteria presented here, and subsequent monitoring of deformation. As population densities increase on the flanks of volcanoes around the world, recognition and prediction of flank failure becomes increasingly urgent. □

Received 3 October 1996; accepted 15 April 1997.

1. Siebert, L. Threats from debris avalanches. *Nature* **356**, 658–659 (1992).
2. Siebert, L., Glicken, H. & Ui, T. Volcanic hazards from Bezymianny- and Bandai-type eruptions. *Bull. Volcanol.* **49**, 435–459 (1987).
3. Denlinger, R. P. & Okubo, P. Structure of the mobile south flank of Kilauea Volcano, Hawaii. *J. Geophys. Res.* **100**, 24499–24507 (1995).
4. van Wyk de Vries, B. & Borgia, A. in *Volcano Instability on the Earth and Other Planets* (eds McGuire, W. J. et al.) 95–110 (Spec. Publ. 110, Geol. Soc., London, 1996).
5. Hradecky, P. *Geologi del Volcán Mombacho* (INETER archives, Managua, Nicaragua, 1987).
6. Sussman, D. Apoyo Caldera, Nicaragua: a major Quaternary silicic eruptive center. *J. Volcanol. Geotherm. Res.* **24**, 249–282 (1980).
7. Borgia, A. The dynamic basis of volcanic spreading. *J. Geophys. Res.* **99**, 17791–17804 (1994).
8. Merle, O. & Borgia, A. Scaled experiments of volcanic spreading. *J. Geophys. Res.* **101**, 13805–13817 (1996).
9. van Bemmelen, R. W. *Mountain Building* (Martinus Nijhoff, The Hague, 1954).
10. Iverson, R. M. Can magma-injection and groundwater forces cause massive landslides on Hawaiian volcanoes? *J. Volcanol. Geotherm. Res.* **66**, 295–308 (1985).
11. Elsworth, D. & Voight, B. in *Volcano Instability on the Earth and Other Planets* (eds McGuire, W. J. et al.) 45–53 (Spec. Publ. 110, Geol. Soc. London, 1996).
12. Moore, J. G. et al. Prodigious submarine landslides on the Hawaiian Ridge. *J. Geophys. Res.* **94**, 17465–17484 (1989).
13. Wadge, G., Francis, P. W. & Ramirez, C. F. The Socompa collapse and avalanche event. *J. Volcanol. Geotherm. Res.* **66**, 309–336 (1995).
14. van Wyk de Vries, B., Self, S. & Francis, P. W. Was Socompa pushed or did it fail? *J. Conf. Abstr.* **2**(1), 78 (1997).
15. van Wyk de Vries, B. & Merle, O. The effect of volcanic constructs on rift fault patterns. *Geology* **24**, 643–646 (1996).
16. Naranjo, J. A. & Francis, P. W. High velocity debris avalanche deposit at Lastarria volcano in the north Chilean Andes. *Bull. Volcanol.* **49**, 509–514 (1987).
17. Chigira, M. Long-term gravitational deformation of rocks by mass rock creep. *Eng. Geol.* **32**, 157–184 (1992).
18. Lopez, D. L. & Williams, S. N. Catastrophic volcano collapse: relation to hydrothermal alteration. *Science* **260**, 1794–1796 (1993).
19. Siebert, L. Large volcanic debris avalanches: characteristics of source areas, deposits, and associated eruptions. *J. Volcanol. Geotherm. Res.* **22**, 163–197 (1984).
20. Reid, M. E. Destabilizing hydrothermal pressurisation in volcanoes. *Abstr. IUGG XXI Assembly* Vol. A, 464 (Int. Un. Geodesy Geophys., Boulder, 1995).
21. Swanson, D., Hausback, B. P. & Zimbelman, D. R. Why was the 1980 Bulge on the North flank of Mount St. Helens? *Abstr. IUGG XXI Assembly* Vol. A, 464 (Int. Un. Geodesy Geophys., Boulder, 1995).
22. Murray, J. B. Ground deformation at Colima volcano 1982–1991. *Geofis. Int.* **32**, 659–670 (1994).
23. Murray, J. B., Voight, B. & Glot, J.-P. Slope movement crisis on the east flank of Mt. Etna volcano: Models for eruption triggering and forecasting. *Eng. Geol.* **38**, 185– (1992).
24. Moore, J. G. & Albee, W. C. *Prof. Pap. US Geol. Surv.* **1250**, 123–141 (1981).
25. Simkin, T. & Siebert, L. *Volcanoes of the World* (Geoscience, Tucson, 1995).
26. Terzaghi, K. & Peck, R. B. *Soil Mechanics in Engineering Practice* 2nd edn (Wiley, New York, 1967).

Acknowledgements. We thank W. Strauch, P. Perez and O. Membrenéz for assistance in the field, and H. Rymer, D. Rothery, D. Peate, F. Garland and P. Bland for reviews. This work was supported by the Leverhulme Trust.

Correspondence and requests for materials should be addressed to B.v.W. d.v. (e-mail: b.van-wyk-de-vries@open.ac.uk).

New evidence concerning avian origins from the Late Cretaceous of Patagonia

Fernando E. Novas* & Pablo F. Puerta†

* Museo Argentino de Ciencias Naturales Bernardino Rivadavia, Av. Angel Gallardo 470, Buenos Aires (1405), Argentina

† Museo Paleontológico Egidio Feruglio, Av. 9 de Julio 655, (9100) Trelew, Argentina

The spate of recent discoveries of Mesozoic birds has substantially improved our understanding of the early evolution of birds and flight^{1–5}, but has failed to close the morphological gap between the Upper Jurassic *Archaeopteryx lithographica*, the earliest known bird, and the Dromaeosauridae, the group of non-avian theropod dinosaurs regarded as most closely related to birds^{6,7}. Here we describe a theropod dinosaur from Patagonia, *Unenlagia comahuensis* gen. et sp. nov., which partially fills this gap. Despite

the relatively late appearance of this dinosaur in the fossil record (Upper Cretaceous), several features of *Unenlagia* are more bird-like than in any other non-avian theropod so far discovered. *Unenlagia* resembles *Archaeopteryx* in the morphology of the scapula, pelvis and hindlimb. But several shared, primitive features of the pubis, ischium and hindlimb proportions suggest that *Unenlagia* may represent the sister taxon of the Avialae (=Aves). The structure of the forelimb suggests that the avian mode of forelimb folding, and the extensive forelimb elevation necessary for powered, flapping flight, was already present in cursorial, non-flying theropod dinosaurs.

Theropoda
Coelurosauria⁷
Maniraptora⁷

Unenlagia comahuensis gen. et sp. nov.

Etymology. *Unenlagia*, Latinized from “uñen” and “lag”, Mapuche Indian names respectively meaning “half” and “bird”⁸; and *comahuensis*, from Comahue, a Mapuche name referring to North-West Patagonia.

Holotype. (See Fig. 1).

Locality and horizon. Upper Cretaceous (Turonian-Coniacian⁹), Río Neuquén Formation, Sierra del Portezuelo, Neuquén Province, Argentina. This formation has yielded remains of the basal bird *Patagonykus puertai*^{10,11}, plus a variety of non-avian theropods¹².

Diagnosis. Possesses tall neural spines in posterior dorsals and anterior sacral vertebrae, being nearly twice the height of the centrum; deep lateral pits in the base of the neural spines of these vertebrae; twisted scapular shaft; inflected dorsal margin of post-acetabular iliac blade (Fig. 2).

Unenlagia is a medium-sized maniraptoran dinosaur, nearly 2 m long. Presacral vertebrae are amphiplatyan and have pleurocoels. Six fused sacrals are present, although the ilia extend the length of at least nine vertebrae (that is, six sacrals, two dorsals, and one caudal), instead of seven as in *Deinonychus* (Museum of Comparative Zoology, MCZ 4871) and *Archaeopteryx*^{13,14}. Proximal haemal arches are craniocaudally short and dorsoventrally long (Fig. 1), resembling those of the dromaeosaurid *Veliciraptor*¹⁵.

The scapula (Fig. 2a, b) is strap-like in dorsal aspect and curved in lateral view, closely resembling that of *Archaeopteryx*^{6,16}. As in the latter, the acromion is triangular in lateral aspect, and projected sharply cranioventrally. In contrast to the situation in non-avian theropods (for example, *Deinonychus*^{16,17}), the humeral articulation of the scapula of *Unenlagia* is laterally oriented as in birds^{6,16,18}.

The humerus, estimated to be 27 cm long, is 71% of the femoral length, and is proportionally shorter than in *Archaeopteryx*^{13,14}. As in other Maniraptora⁷, the internal tuberosity (bicipital crest of modern birds¹⁹) is proximodistally extended.

The pelvic bones are not fused (Fig. 2c). The ilium is extensive cranially, but the postacetabular blade is short. The latter is low and sharp as in *Archaeopteryx* and enantiornithines^{14,20}. The fossa for the m. cuppedicus is well developed, a condition that is widely present among Coelurosauria, including basal birds^{10,17,18}. In contrast to non-avian coelurosaurians (that is, *Deinonychus*^{17,21}), the acetabulum of *Unenlagia* tends to close off medially, resembling *Archaeopteryx*⁸, *Patagonykus*²² and hesperornithiforms^{23,24}. The brevis fossa is considerably more reduced than in *Deinonychus*¹⁰. The pubis is slightly shorter than the femur, is oriented ventrally as in other maniraptorans^{10,14}, and distally bears a caudally projected ‘foot’. The pubic shaft expands transversally into a ‘pubic apron’ (Fig. 2d) that is widely extended proximodistally as in *Deinonychus* (MCZ 4371), but in contrast with the more reduced symphysis of *Archaeopteryx* and more derived birds^{6,11}. The ischium is a short, plate-like bone, triangular in side view. The obturator notch is enclosed distally by a triangular obturator process, a primitive condition lost in *Archaeopteryx*^{6,14} and more derived birds^{11,22}. However, the dorsal edge of the ischium exhibits a prominent proximodorsal process (Fig. 2c), separated from the ischiadic